Proceedings of the 30th International Cosmic Ray Conference
Rogelio Caballero, Juan Carlos D'Olivo,
Gustavo Medina-Tanco, José F. Valdés-Galicia (eds.)
Universidad Nacional Autonóma de México,
Mexico City, Mexico, 2009
Vol. 6, pages 225-237

30TH INTERNATIONAL COSMIC RAY CONFERENCE

Sun, Corona, and Transient Phenomena in the Heliosphere

BERNDT KLECKER
Max-Planck-Institut für extraterrestrische Physik, Garching, Germany
berndt.klecker@mpe.mpg.de

Abstract. This rapporteur paper addresses the sessions SH 1 *Sun and Corona* (SH 1.2 – SH 1.7) and SH 2 *Transient Phenomena in the Heliosphere* (SH 2.1 – SH 2.4) of the 30^{th} International Cosmic Ray Conference (ICRC) that took place at Merida, Mexico during July 3 – 10, 2007. Session SH 1 includes solar emissions from energetic photons and electrons to solar neutrons, and the acceleration and transport of energetic charged particles at the Sun and in interplanetary space. Session SH 2 covers transient phenomena in interplanetary space and includes the effects of coronal mass ejections, corotating and merged interacting regions, and travelling interplanetary shocks.

Introduction

This rapporteur paper covers the sessions SH 1, Sun and Corona (SH 1.2-1.7), and SH 2, Transient Phenomena in the Heliosphere (SH 2.1-2.4). These 10 sessions are re-grouped into 9 topics, basically following the structure of the individual sessions. Table 1 shows a summary of the sessions and the statistics of papers. It is evident from the total number of 92 papers presented in these sessions, that this rapporteur paper cannot cover all sessions completely. It is rather the intention to provide an overview of the progress in this field and to concentrate on representative highlights, new findings, and future perspectives.

Session	Topic	Oral	Poster	Total
SH 1.2	Photons+Electrons	4	2	6
SH 1.3	Solar neutrons	3	6	9
SH 1.4	SEP spectra	10	3	13
SH 1.5	Part. Accell.	3	1	4
SH 1.6	Interpl. Transp.	8	9	17
SH 1.7	CMEs	2	6	8
SH 2.1	Forbush decrease	13	10	23
SH 2.2	CIRs	1	3	4
SH 2.3	Prop. Interact.	2	5	7
SH 2.4	MIRs	0	1	1
Total		46	46	92

Table 1. Paper Statistics.

Sun and Corona

Energetic Photons and Electrons

The electromagnetic emission provides direct information on the temporal profiles and energy spectra of accelerated electrons and ions in solar flares. Over the last years many missions became available that provide detailed measurements of the electromagnetic emission, including, for example, CGRO, Coronas-F, GOES, INTEGRAL RHESSI, SOHO, and TRACE. Several authors reported at this conference new results using hard X-ray and γ-ray data from the γ-ray spectrometer SPI onboard INTEGRAL (International Gamma Ray Astrophysics Laboratory) and from the SONG (Solar Neutrons and Gamma-rays) instrument of the Coronas-F spacecraft. SPI covers hard X-rays and γ-rays in the energy range $\sim$ 20 keV to 8 MeV [73], and SONG / CORONAS-F covers hard X-rays and γ-rays in the energy range 0.03 – 100 MeV, neutrons in the energy range $\sim$7-100 MeV and high energy protons ($>$ 70 MeV) and relativistic electrons ($>$ 55 MeV) [1, 37, 38].

Struminsky et al. [65], using data from the Anticoincidence Subsystem (ACS) of SPI (hard X-rays $>$ 150 keV), analyzed the time profiles of sev-

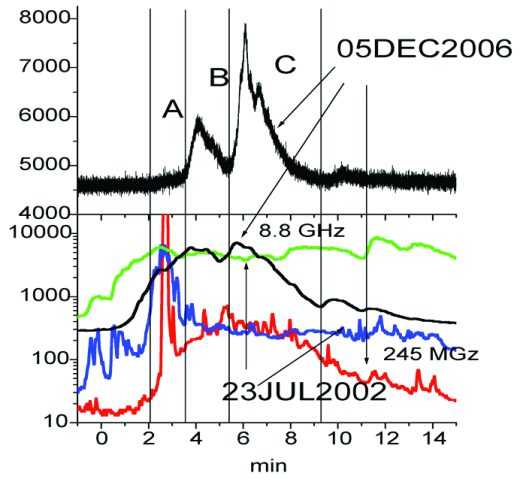

Fig. 1. The time profile of the ACS/SPI count rate (top), and the radio emission at 245 MHz and 8.8 GHz (bottom) for the December 5, 2006 event [65].

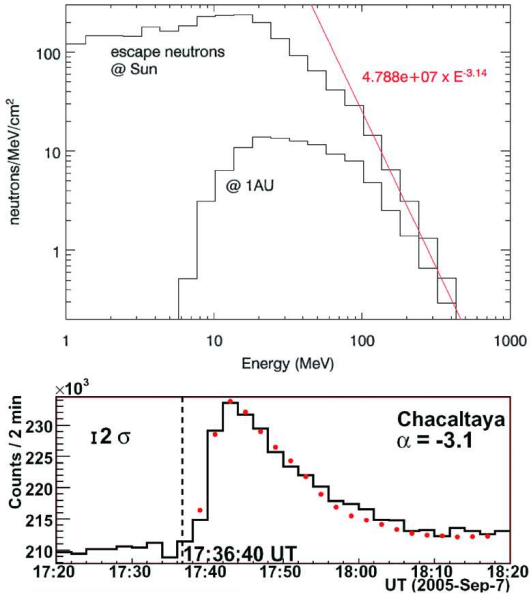

Fig. 2. Simulated neutron spectra for the September 7, 2005 event (top) and comparison with observations (bottom) [76].

eral X-class flares in December 2006. They found during the impulsive phase of these events multiple peak structures in the hard X-ray emission (1), consistent with several phases (A, B, C) related to dominant continuum (A), dominant γ-ray line emission (B), and decay (C) (s.a. [27]), with hard X-ray emission in phases B and C., and effective proton acceleration in C.

INTEGRAL/SPI observations of the time profile of the neutron capture line at 2.223 MeV for the October 28, 2003 X17.2/4B solar flare [27] have been used to infer the density profile in the photosphere. Assuming stochastic acceleration and using the time profile of the nuclear de-excitation lines in the energy range 4.1-6.4 MeV (^{12}C+^{16}O) as a proxy for the time history of initial neutron production in the energy range 1 – 100 MeV, Troitskaia et al [66] inferred with their neutron propagation code an increased photospheric density ($\sim$2 10^{17}cm^{-3}), consistent with previous results in other flare events [67].

An extended source of gamma-emission produced by inverse-Compton scattering of cosmic-ray electrons by the radiation field of the Sun was studied by Orlando et al. [55]. They found consistency between the model predictions and EGRET observations at $>$ 100 MeV. With the much improved sensitivity (factor $>$ 30) of GLAST (Gamma-Ray Large Area Telescope) scheduled for launch in 2008, the extended inverse–Compton γ -ray emission may be readily used in the future to infer the cosmic ray electron spectra in the inner heliosphere, close to the Sun.

Solar Neutrons

High energy solar neutrons provide direct information on the mechanisms that accelerate particles at the Sun to high energies. Neutron observations have the advantage of not being affected by propagation effects in turbulent magnetic fields, propagating rectilinear from the acceleration site at the Sun to the point of observation at Earth or in interplanetary space. High-energy neutrons are measured by neutron monitor (NM) stations distributed around the Earth and, since solar cycle 23, by a number of neutron telescopes (SNT) (e.g.[46]). The large number of X-class flares in 2005 and 2006 provided the unique opportunity to search systematically for high energy neutron signatures using SNTs, however, significant counting rates were only observed in association with the X17.0 flare on September 7, 2005 [47]. This event was studied in detail by several authors using both γ-ray and neutron observations [19, 64, 76].

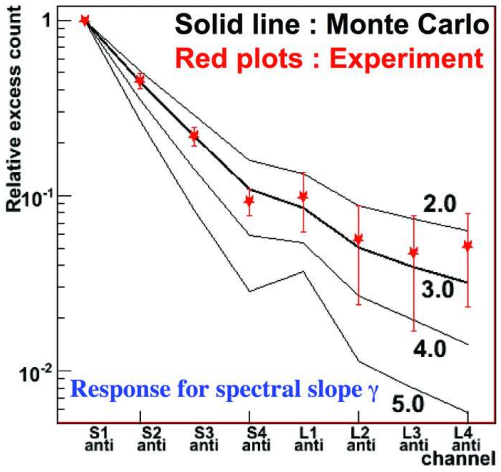

Fig. 3. Simulated neutron spectra for spectral slopes of 2, 3 add 4 and measurement [64].

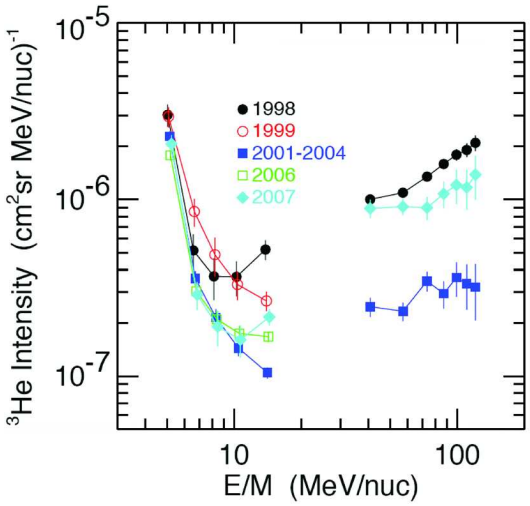

Fig. 4. ^{3}He spectra during quiet times (left) and GCR spectra (right) for several time periods between 1998 and 2007, covering solar maximum and solar minimum conditions [80].

Watanabe et al. [76] derived a power law index of $\gamma = -3.1$ (Fig. 2) for the energy spectrum of the injected neutrons by fitting the time profile of the neutron counting rate observed by the Chacaltaya NM, assuming power law injection spectra, and an injection time profile as observed for the 4.4 MeV γ-ray line emission by the INTEGRAL satellite. Then, using the neutron spectrum and Hua's loop model [22] they derived a power law index of -3.6 for the spectrum of accelerated ions.

SNT measurements with their ability to determine the energy of the neutrons provide an independent method to derive the energy spectra of energetic neutrons at the Sun. The energy dependent response of SNTs allows to infer the injection spectrum directly, comparing the counting rates in different energy channels with Monte Carlo simulations. Sako et al. [64] obtained for the September 7, 2005 event with this method for the injected neutron spectrum a value of $\gamma \sim -3$ (Fig. 3), compatible with the results of Watanabe et al. [76], shown in Fig. 2.

The simultaneous detection of high-energy neutrons and protons with energies exceeding 10 GeV [53]in association with the April 15, 2001 flare puts interesting constraints on acceleration models.

Energetic Charged Particle Spectra, Composition and Charge States

The energy spectra, elemental, and isotopic abundances, and ionic charge composition of solar energetic particles (SEP) carry fundamental information on the source region and their acceleration and propagation processes. These signatures, together with signatures on the electromagnetic emission, have been used in the past to classify SEP events as impulsive and gradual. In this scenario the ^{3}He- and heavy ion-rich impulsive SEP events were related to flares, showing also high ionic charge states of Fe. The gradual SEP events were related to coronal mass ejection (CME) driven coronal and interplanetary shocks with elemental abundances and ionic charge states similar (although not identical) to those in the solar wind (e.g. [60]). However, new results from instruments with improved collecting power and resolution onboard several spacecraft (e.g WIND, SAMPEX, SOHO, ACE) have shown that this two–class picture was oversimplified (for recent reviews see, e.g., [7, 28]). The new composition and ionic charge measurements show that enrichments in ^{3}He at $\sim$1 MeV/nuc are also common in interplanetary shock accelerated populations [12], suggesting a suprathermal population from previous

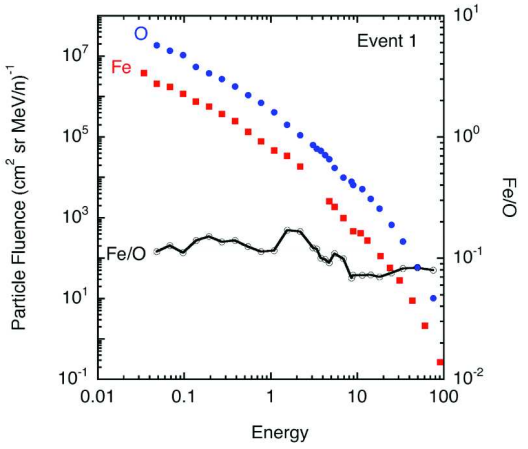

Fig. 5. Energy spectra of O and Fe, and Fe/O-ratio in the 8 December, 2006 SEP event [10].

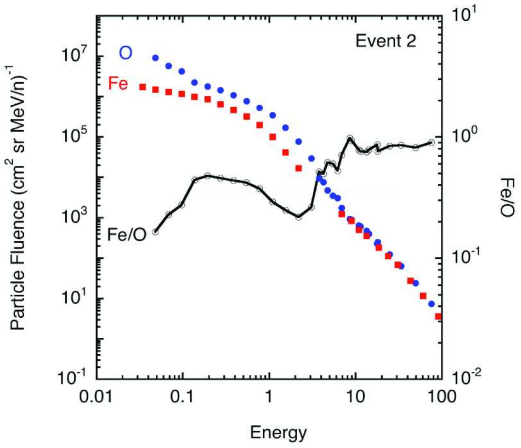

Fig. 6. Energy spectra of O and Fe, and Fe/O-ratio in the 14 December, 2006 SEP event [10].

'impulsive' events [44] as the source. The observation that during solar maximum ^{3}He in the energy range 0.2-16 MeV/nuc was observed at 1AU $>$60% of the time [79], and that this component is dominated at low energies even during solar minimum by a solar component from unresolved impulsive ^{3}He-rich SEP events (Fig.4, [80]), strongly supports this view. At high energies, on the other hand, enrichments of heavy ions are often observed in large events, with high charge states at high energies [58].

There are presently basically two different scenarios discussed to explain the new complexity of observations that deviate from the simple two-class picture. Scenario 1 assumes direct injection of particles from the flare acceleration process (e.g. [6], [31] , and references therein), with or without further acceleration by a coronal shock. In Scenario 2 these new findings are interpreted as the interplay of shock geometry and different seed populations, i.e. solar wind and flare suprathermals, the latter with their higher energy being preferentially injected at a perpendicular shock [69, 70]. These scenarios are now heavily debated and were also discussed in several papers at this conference.

Cane et al. [8] presented an update of Scenario 1 that could qualitatively explain the new observations by invoking three phases of particle acceleration and two conditions for detecting these particles in interplanetary space. The three phases being the flare impulsive phase (1), the flare late phase (2), and shock acceleration (3). The two conditions needed are open field lines and magnetic connection between the point of observation and the acceleration site. In the scenario put forward by Tylka et al. [69] high Fe abundances and high charge states of Fe at energies $>$ 10 MeV/nuc are explained by the combined effect of two seed populations (coronal and heavy ion rich flare material, the latter with a high mean charge of Fe) and higher injection efficiency of the already pre-accelerated flare population at a perpendicular shock [69, 70].

Cohen et al. [10] tested the different scenarios with two large events from the same active region, observed in December 2006 with ACE and STEREO, originating at $\sim$E70 and $\sim$W25, respectively. Both events were accompanied by quasi-parallel interplanetary shocks arriving at 1 AU on December 8 and 14, respectively. These two large SEP events showed significantly different heavy ion abundance signatures (Fig.5 and Fig.6), with high Fe/O–ratios at high energies for the second event originating at $\sim$W25. Assuming the same acceleration conditions in these two events, the large difference of the Fe/O ratio would be more consistent with Scenario 1, because condition 2 of Scenario 1, i.e. good connection to the acceleration site, is more likely to be fulfilled for event 2 originating at W25.

However, the characteristics of the CME driven shocks close to the Sun (i.e. quasi-parallel or quasi-perpendicular) are not (yet) observable and

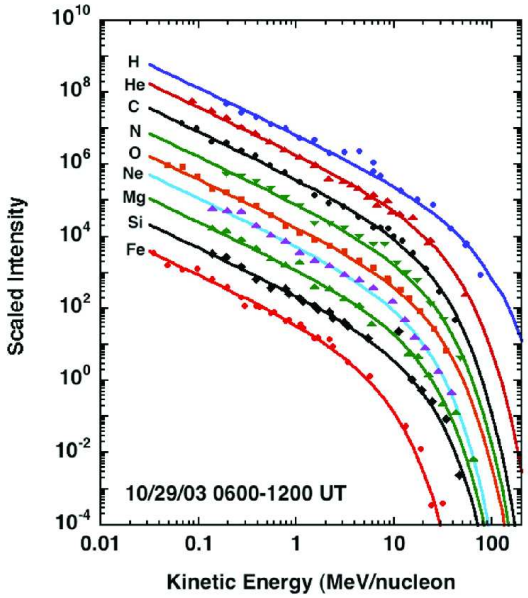

Fig. 7. Energy spectra following the arrival of a shock on October 29, 2003. At high energies the spectra show the typical M/Q-dependent roll-over [48].

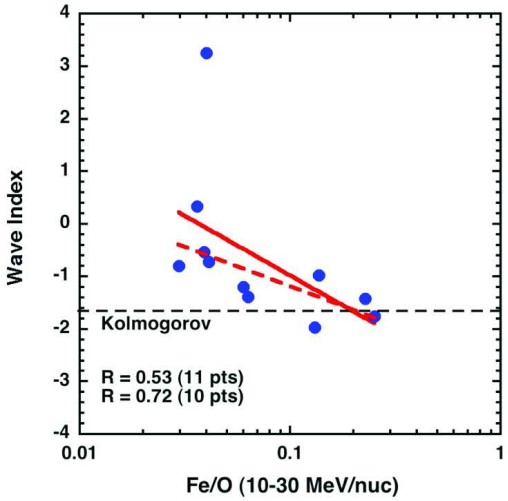

Fig. 8. Plot of The interplanetary wave index q (P(k)$\sim$ k^{-q}), deduced from the Q/M-dependence of E_0, assuming that the spectral brakes are governed by diffusion processes [48].

thus Scenario 2 cannot be excluded from this measurement. The first measurements of SEPs with STEREO in December 2007, demonstrating the excellent performance of the STEREO instrumentation and the very good agreement with data from ACE [49, 75], showed that more conclusive results may become available in the near future when measurements of the same SEP event with several spacecraft will become available at separation distances sufficiently large to test the influence of different connection longitudes.

Energy Spectra and Composition

The new instruments with high sensitivity available during solar cycle twenty three provide SEP energy spectra for many elements over the wide energy range of $\sim$0.1 – 100 MeV/nuc. These observations revealed that most large (gradual) SEP events have power law spectra at low energies, with spectral breaks at high energies that often can be approximated by

$$dJ/dE = kE^{-\gamma}\exp(-E/E_0),$$

where E is the kinetic energy per nucleon, k and γ are constants and E_0 generally depends on the mass (M) and charge (Q) of the ions as

$$E_0 = E_{0p} \times \left(\frac{\mathrm{Q}}{\mathrm{M}}\right)^{\beta},$$

and E_{0p} is the e-folding energy of protons (e.g. [68], and references therein).

Fig.7 [48] shows as an example the energy spectra of H – Fe ions for the October 29, 2003 interplanetary shock related SEP event. It is obvious that the e-folding energy depends strongly on M/Q. In a statistical study of 11 large events Mewaldt et al [48] investigated the Q/M dependence of E_0 and correlated the Q/M power-law exponent β with various parameters. They found that β is correlated with the proton fluence at $>$10 MeV and the low-energy power-law slope γ, and anti-correlated with the Fe/O-ratio at 10-30 MeV/nuc.

Assuming that the location of the spectral breaks in fluence spectra is governed by diffusion processes [9], and that the diffusion coefficient scales with particle rigidity (R) as R^{α}Q/M power-law index β can be related to the local turbulence spectrum of the magnetic field P (k) $\sim k^{-q}$, assumed to be a power law in wave number k. Fig. 8 shows the power-law index of the wave turbulence as a function of the Fe/O-ratio. This result indicates that there is additional turbulence

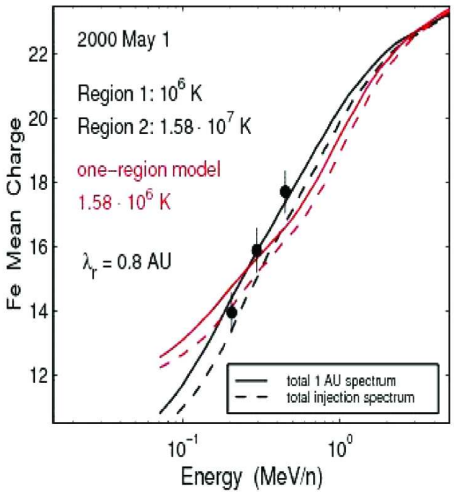

Fig. 9. Observed Fe ionic charge (filled circles) and calculated spectrum of Fe at 0.05 AU (injection spectrum, dashed line) and at 1 AU after interplanetary transport (solid line), assuming a constant interplanetary scattering mean free path of λ=0.8 AU [26].

(flat turbulence spectra with q$\sim$0) near the interplanetary shock in those events with small Fe/O-ratio and large proton fluence, consistent with the scenario of additional proton-generated waves near the shock that are scattering the heavy ions [54]. These additional wave turbulence has, indeed, been observed in some events with particularly high intensity of low-energy ions near the interplanetary shock (e.g. [2]).

Charge States

Within the last $\sim$10 years measurements with improved instrumentation on the SAMPEX, SOHO and ACE spacecraft provided ionic charge states in SEP events over an extended energy range from $\sim$0.1 to 80 MeV/nuc (for Fe). These measurements revealed that heavy ion charge states generally depend on energy and they showed a large variability of the energy dependence, most pronounced for Fe ions (see e.g. [29] for a recent review). The ionic charge states show significantly different signatures for interplanetary shock related events and ^{3}He- and Fe-rich events. Whereas in all ^{3}He-rich events observed so far the ionic charge increased from $\sim$14–16 at 180–250 keV/nuc to $\sim 16-20$ at $350-550$ keV/nuc [50]. Klecker et al. [30] reported at this conference the results of a statistical study of the ionic charge of Fe in 35 IP shock related events. They showed that in 32 out of these 35 events the ionic charge of Fe did not vary significantly with energy in the energy range 0.18 – 0.43 MeV/nuc, with an average ionic charge of Fe of $\sim$10 – 11 at $\sim$0.2 MeV/nuc, similar to typical charge states in the solar wind [32] or at suprathermal energies [5]. The large increase of the mean ionic charge in the energy range $\sim$0.1–0.5 MeV/nuc as observed in ^{3}He- and Fe-rich events can be explained by additional ionization in a dense environment in the low corona (e.g. [25; 33]. For a quantitative comparison of the measured charge spectra with acceleration models, the energy loss by adiabatic deceleration during transport to 1 AU has to be taken into account [25], that shifts the charge spectra to lower energies. It was shown by Kartavykh et al. [26] at this conference that this energy loss is significant, even for propagation conditions equivalent to a large scattering mean free path $\lambda \sim 0.8$ AU, and that for a satisfactory fit of the measured charge spectra of Fe contributions from two regions with different temperature and acceleration conditions are necessary (Fig.9, [14, 26]).

SEP Acceleration and Transport

The observed characteristics of SEP events as described in the previous chapters provide the boundary conditions for modelling the acceleration process. It is now generally accepted that there are several different processes involved, e.g. acceleration processes that involve either stochastic acceleration by plasma wave turbulence (second order Fermi process), acceleration by travelling coronal or interplanetary shocks (generally referred to as shock acceleration, a first order Fermi process), or electric fields. Several papers at the conference discussed these processes. One set of models tries to reproduce heavy ion energy spectra as observed in interplanetary space by modelling acceleration by CME-driven interplanetary shocks [42]. Other models evaluate spectra as expected from the acceleration by stochastic non-Gaussian electric fields [82], and compare the energy as expected from stochastic acceleration, acceleration at a neutral current sheet and shock acceleration [57].

An important aspect for the comparison of the timing of X-rays and γ-rays with the observations

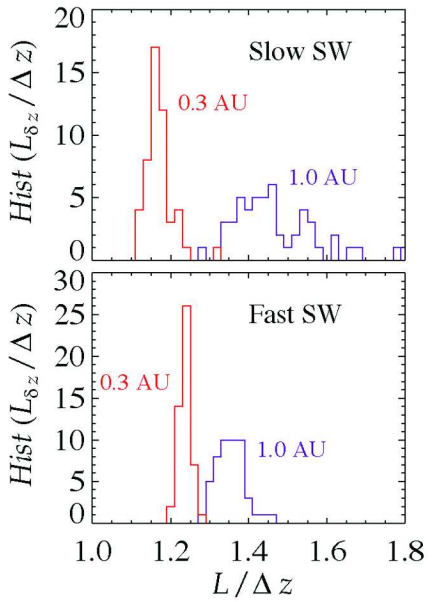

Fig. 10. Ratio L/Δz, or field line lengthening factor, at a resolution scale of δz=10^9 cm, for fast and slow solar wind [59].

of electrons and ions in interplanetary space is to infer their injection time profile at the Sun. The standard technique to deduce the onsets of SEP solar injection times is to plot the arrival times t_{arr}

$$t_{arr} = t_{SRT} + L_{spiral}/v$$

(e.g. [28] and references therein), assuming an energy-independent solar release time t_{SRT} and for the first particles scatter-free propagation along the average Parker-spiral interplanetary magnetic field of length L_{spiral}. Ragot and Kahler [59] investigated the lengthening of the magnetic field lines due to turbulence on various length scales and found that the length of the field lines can be considerably increased, in slow solar wind at 1 AU and for turbulence scales of 10^9 cm by about 50% (Fig.10). This effect could change travel delays considerably, for example for 10 MeV protons in slow solar wind by ∼20 min. In their simulations they do not get field lines shorter than L_{spiral}, in contrast to the results of Pei et al. [56].

At higher energies the relative timing of high energy protons inferred from neutral pion decay and the observation of relativistic protons with neutron monitors on Earth is not as severely influenced by propagation effects. Timing results for the large GLE events on October 28, 2003 and January 20, 2005 showed that in these events the high energy particle population responsible for the γ-rays and neutrons at the Sun and for the GLE onset on Earth belonged to the same population, accelerated in close connection to the flare process [39].

The only way to avoid ambiguities introduced by the implicit assumption that the first arriving particles do not encounter any scattering, is to solve the full transport equation, and to use the intensity-time and anisotropy-time profiles to infer the injection time profile ([14], [43]).

An important parameter in these models is the pitch angle diffusion coefficient ($D_{\mu\mu}$) and its relation to the fluctuations of the magnetic field in the solar wind. Dröge et al. [15] used numerical solutions of the focused transport equation with diffusion coefficients based on dynamical quasilinear theory (DQLT). The inclusion of the dissipation range and dynamical effects in DQLT lead to large differences of the μ-dependence of $D_{\mu\mu}$ compared to QLT, distinctly different for protons and electrons at energies less than a few MeV (e.g. [13], and references therein). This results at low energies, compared to QLT, in a significantly larger scattering mean free path for electrons and only moderate changes for protons, consistent with observations (Fig.11). The model calculations show that the parallel transport of solar particles in impulsive events can be explained well by DQLT and slab / 2D decomposition of magnetic fluctuations (typically ∼20% slab, ∼80% 2D fluctuations). However, the electron pitch angle distributions are typically not consistent with forms of $D_{\mu\mu}$ predicted by DQLT, suggesting the importance of non-linear effects that need further investigation [15].

Coronal Mass Ejections

The near-Earth observations with several spacecraft including Wind, SOHO and ACE resulted during the last ∼10 years in a large number of observations of coronal mass ejections (CME) and interplanetary coronal mass ejections (ICMEs), where ICMEs are the interplanetary manifestations of coronal mass ejections observed by coronographs near the Sun. Fig.12 shows a schematic picture of the three-dimensional structure of an ICME

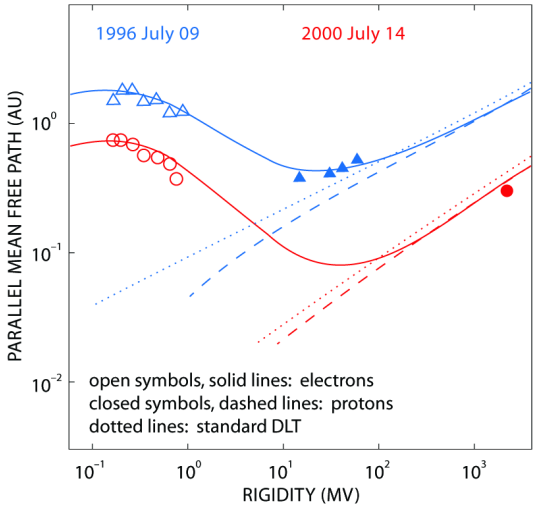

Fig. 11. Mean free path obtained from particle observations and predictions for protons and electrons from DQLT [15].

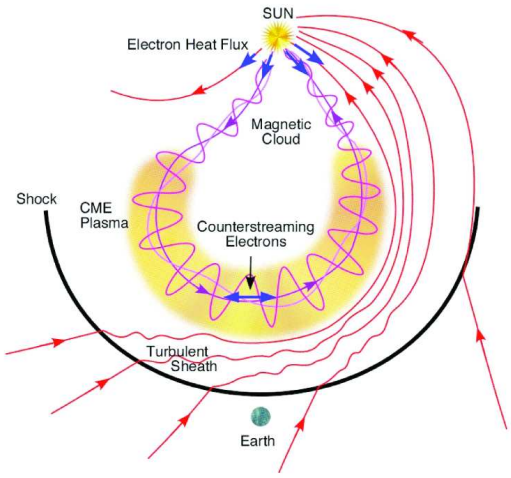

Fig. 12. Schematic of the three-dimensional structure of an ICME with upstream interplanetary shock, relating plasma and magnetic field signatures (from [83]).

and upstream shock, indicating some of the in-situ signatures (magnetic field, plasma, bi-directional electrons) of this structure. There are a large number of plasma and magnetic field signatures and effects associated with CMEs and ICMEs (e.g. [83], and references therein), some of them have been discussed in sessions SH 1.7, SH 2.1, and SH 2.3 at this conference as summarized below.

The effects associated with CMEs and ICMEs include the generation of coronal and interplanetary shocks [20], which may accelerate particles [34], geomagnetic storms, when the ICME is interacting with the magnetosphere of the Earth [81], and short-term decreases in the galactic cosmic ray intensity (Forbush decrease, see next section). Some properties of ICMEs as observed in the ecliptic and at high latitudes have been summarized by Richardson and Cane [61]. Fig. 13 shows as an example (from top to bottom) the ICME rate near Earth, the monthly sunspot number, the percentage of magnetic clouds, the ICME and mean ICME speed, and the ICME rate at Ulysses. The results show that the average ICME rate at Ulysses is comparable to that at Earth ($\sim$ 2/solar rotation), despite the variations in spacecraft latitude.

The correlation between expansion speed and radial speed of CMEs was investigated by Muñoz et al. [52]. Using limb CMEs where both the radial speed (V_{rad}) and the expansion speed (V_{exp}) can be directly determined they showed that for CMEs with an opening cone of $< 90°$ the empirical relation V_{rad} = 0.88 V_{exp} found by DalLago et al. [11] can be generalized by introducing the angular width or cone angle, providing an estimate of the expansion speed for off-limb CMEs.

A subset of ICMEs characterized by enhanced magnetic field strength and with a smooth rotation of the magnetic field direction is referred to as magnetic clouds. The topology of the magnetic field inside the magnetic cloud can be inferred from a comparison of the in-situ measurements of the magnetic field and plasma parameters with a model. One basic structure usually assumed for these models is a large loop (flux rope), locally described by a cylinder with circular cross section, with the magnetic field lines wrapped around the axis of the flux rope (see schematic in Fig.12). Vandas et al. [72] showed the results of a generalization of these models introducing an elliptical cross section of the ICME. This generalization resulted for several cases in a considerably improved fit of the magnetic field measurements.

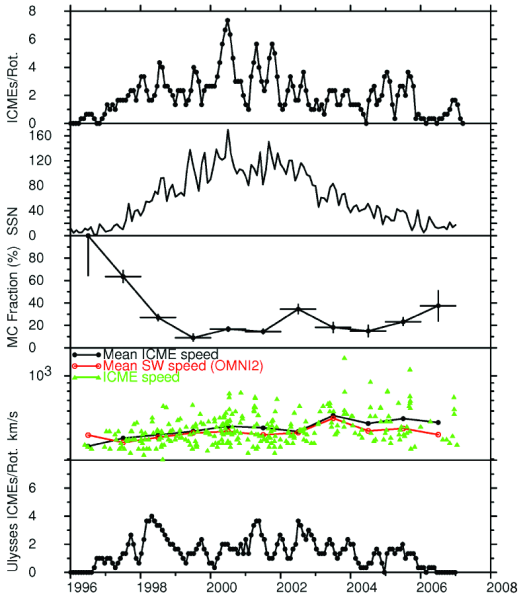

Fig. 13. (From top): ICME rate per solar rotation at the Earth, monthly sunspot number, fraction of ICMEs that are magnetic clouds, mean ICME and solar wind speeds, and the ICME rate at Ulysses [61].

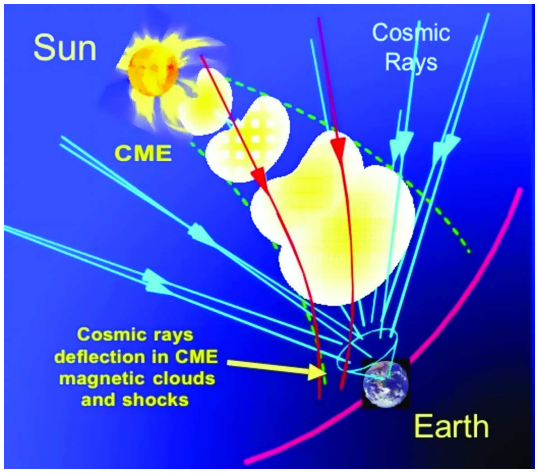

Fig. 14. Schematic of an ICME between Sun an Earth, illustrating the deflection of galactic cosmic rays, thus causing a Forbush decrease (from the prsentation of [3].)

Transient Phenomena in the Heliosphere

Transient phenomena in the heliosphere were the topics of session SH 2.1 to 2.4 at this conference, covering Forbush decreases, the effects of CMEs (SH 2.1), corotating interaction regions (SH 2.2), propagating interaction regions / interplanetary shocks (SH 2.3) and merged interaction regions (SH 2.4).

ICMEs and Modulation

Transient decreases in the cosmic ray count rate lasting typically several days were first observed by Forbush [18]. There are two basic types: non-recurrent decreases caused by transient interplanetary events that are related to interplanetary coronal mass ejections and interplanetary shocks, and recurrent decreases related to corotating interaction regions (CIRs) [62],[77]. The non-recurrent decreases are characterized by a rapid reduction (on the time scale of hours) in cosmic ray intensity, followed by a slow recovery, typically lasting about several days at 1 AU. The maximum reduction as observed by the worldwide neutron monitor stations is $\sim$ 3 - 20%, depending on energy (or latitude) (e.g. [78], and references therein). A schematic illustrating the deflection of cosmic rays by a CME between Sun and Earth, thus causing a Forbush decrease is shown in Fig.14 [3].

In session SH 2.1 several characteristics of the Forbush decreases (FD) have been discussed, including their correlation with solar activity [23] and interplanetary shocks [74], the energy dependence of the recovery time scale [71], and long term solar modulation of galactic cosmic rays [40]. Lara et al. [40] found during the A$>$ 0 cycle of solar activity (the northern polar magnetic field pointing outward) a better correlation of the modulation of cosmic rays with high latitude CMEs than with low latitude CMEs, in agreement with cosmic ray transport theory that predicts for the A$>$0 cycle inward drift of GCRs from the polar regions [24].

Muon hodoscopes, providing muon measurements at GeV energies as a function of zenith and azimuth angles with a typical resolution of 1°-2°, allow to reconstruct the 2-D dynamics of the Forbush decrease. As an example, Fig.15 shows the development of the muon anisotropy at E $>$ 2.3 GeV after the event on December 14, 2006 as measured with the URAGAN hodoscope (cutoff rigid-

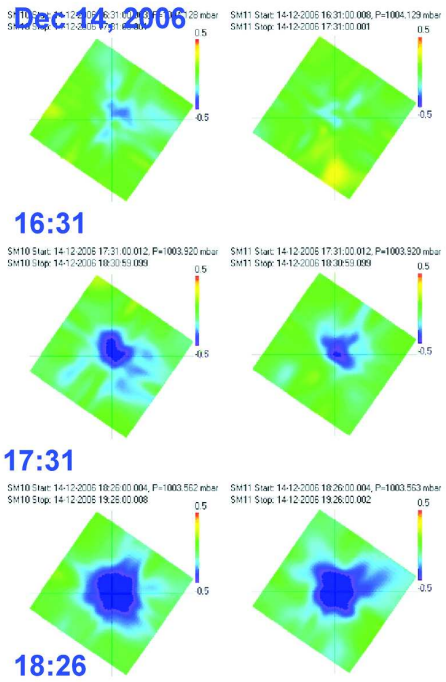

Fig. 15. 2D-dynamics of the muon flux during the Forbush decrease of December 14, 2006 [3].

ity 2.4 GV). The colour code represents excess and deficit of muons from a certain direction [3].

Furthermore, the galactic cosmic ray density and anisotropy information inferred from the ground-based muon detector network can be used to infer ICME geometry and orientation. Using an expanding and convecting cylinder model for the ICME and following the approach of Bieber and Evenson [4], it was demonstrated by Kuwabara et al. [35] that this method resulted for several ICMEs observed during 2003 to 2005 in similar values for ICME orientation and geometry as the analysis of the in-situ determined plasma and magnetic field parameters. This suggests that the cosmic ray based method may be used in the future in a near real time analysis for space weather forecasting systems, as intended, for example, with new muon telescopes as MuSTAnG (Muon Spaceweather Telescope for Anisotropies at Greifswald) [21].

It was also demonstrated that high-energy instruments like the Milagro TeV ground-level γ-ray telescope [63] or IceTop, an air shower array under construction at the South Pole [36] can detect Forbush decreases and thus provide information on complex interplanetary disturbances in the heliosphere.

Corotating Interaction Regions

Corotating interaction regions (CIRs) form when high speed solar wind from coronal holes interacts with the preceding slow solar wind. Forward and reverse shocks accelerate ions to $\sim$MeV energies with peak intensities at several AU, where the forward and reverse shocks are thought to form. Fig.16 shows as an example energetic ions in the energy range $\sim$0.1-2.2 MeV at $\sim$1 AU observed with the two STEREO spacecraft (panel 2, from top), and solar wind parameters for a series of CIRs in early 2007 [51].The figure shows the CIR-related intensity increase of energetic ions, and, at the lowest energy, short-duration spikes originating presumably at the Earth' bow s shock [51].

The composition as observed in CIR accelerated ions indicates contributions from two sources, the solar wind and pick up ions. However, there are several puzzling observations that so far could not be satisfactorily explained (e.g. [45], and references therein). These observations include anomalies of the elemental abundances; for example, He, C, and Ne abundances, relative to oxygen, are significantly larger than in the solar wind and the C/O-ratios in CIRs vary by a factor of $\sim$2-3 with solar wind velocity. Another puzzle is the strong non field aligned transport at times of maximum intensity near 1 AU, compatible with large perpendicular diffusion [17].

With STEREO new multi-spacecraft measurements of CIR energy spectra, composition, and anisotropies covering the energy range from suprathermal energies to $\sim$10 MeV/nuc are now becoming available [41], that will help to solve some of the puzzles in the near future.

CIRs also act as a diffusive barrier for the transport of particles into the inner heliosphere. Long-term modulation of GCRs observed by IMP-8 for four solar cycles showed that recurrent cosmic ray depressions due to CIRs are larger in A$>$0 solar cycles than in A$<$0 solar cycles, inconsistent with the expectation that the cosmic rays entering the inner heliosphere during the A$<$0 solar cycle along the heliospheric current sheet will be more strongly

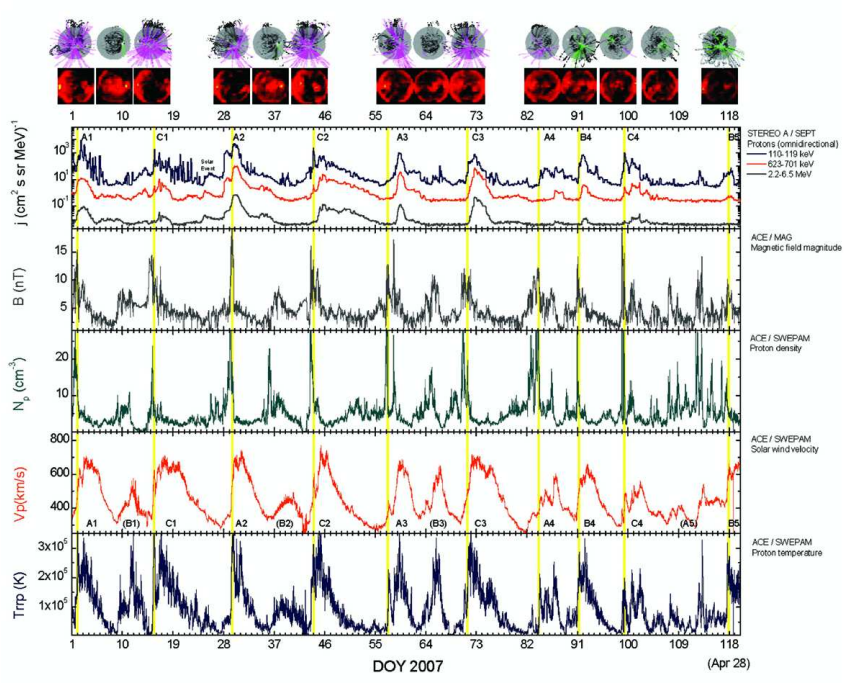

Fig. 16. A series of CIR events as observed by STEREO (top panel) and ACE in early 2007 [51].

modulated. [62]. It was also shown that Jovian electrons in the energy range ∼2.5-10 MeV as observed by Ulysses at heliographic latitudes $<30^{\circ}$ were efficiently modulated by CIRs [16].

Summary and Outlook

In Sessions SH 1 and SH 2 of the 30^{th} ICRC at Merida, Mexico that are covered in this Rapporteur paper a number of exiting results have been presented as summarized above. Where will we go next?

With the solar activity expected to pick up between this and the next ICRC in 2009, we expect to get both, remote-sensing and in-situ multi-spacecraft measurements of flares, CMEs and interplanetary shocks. New observations with the two STEREO spacecraft and other missions near L1 (e.g. ACE, SOHO) will enable us for the first time to tackle the problem of a 3-D reconstruction of CMEs. The new measurements, combined with modelling of the propagation of CMEs and ICMEs, and of particle acceleration will certainly improve our understanding of these energetic phenomena in the inner solar system.

Acknowledgements

The author is grateful to the organizers of the $30^{\rm th}$ ICRC in Merida, Mexico for the invitation to present a rapporteur paper and for their hospitality.

References

[1] I.V. Arkhangelskaja et al., Proceedings of the 30th ICRC, Mérida, México, 2007, Vol. 6, p. 15.
[2] K. Bamert et al., Astrophys. J. 601 (2004) L99.
[3] N.S. Barbashina et al., Proceedings of the 30th ICRC, Mérida, México, 2007, Vol. 1, p. 315.
[4] J.W. Bieber and P. Evenson, GRL 25 (1998) 2955.
[5] A.T. Bogdanov et al., Adv. Space Res. 30 (2002) 111.

[6] H.V. Cane et al., Geophys. Res. Lett. 30 (2003) 8017.
[7] H.V. Cane and D. Lario, Space Science Rev. 123 (2006) 45.
[8] H.V. Cane et al., Proceedings of the 30th ICRC, Mérida, México, 2007, Vol. 1, p. 67.
[9] C.M.S. Cohen et al., J. Geophys. Res. 110 (2005), doi:10.10029/2004JA011004.
[10] C.M.S. Cohen et. al., Proceedings of the 30th ICRC, Mérida, México, 2007, Vol. 1, p. 95.
[11] A. DalLago et al., Adv. Space Res. 32 (2003) 2637.
[12] M.I. Desai et al., Astrophys. J. 553 (2001) L89.
[13] W. Dröge, Astrophys. J. 589 (2003) 1027.
[14] W. Dröge, et al., Astrophys. J. 645 (2006) 1516.
[15] W. Dröge, and Y.Y. Kartavykh, Proceedings of the 30th ICRC, Mérida, México, 2007, Vol. 1, p. 159.
[16] P. Dunzlaff et al., Proceedings of the 30th ICRC, Mérida, México, 2007, Vol. 1, p. 363.
[17] J.R. Dwyer et al., Astrophys. J. 490 (1999) L115.
[18] S.E. Forbush, Phys. Rev. 51 (1937) 1108.
[19] L.X. Gonzalez et al., Proceedings of the 30th ICRC, Mérida, México, 2007, Vol. 1, p. 57.
[20] J.A. Gonzalez-Esparza et al., Proceedings of the 30th ICRC, Mérida, México, 2007, Vol. 1, p. 393.
[21] R. Hippler et al., Proceedings of the 30th ICRC, Mérida, México, 2007, Vol. 1, p. 347.
[22] X.-M. Hua et al., Astrophys. J. Suppl. 140 (2002) 563.
[23] M. Jain et al., Proceedings of the 30th ICRC, Mérida, México, 2007, Vol. 1, p 295.
[24] J.R. Jokipii, E.H. Levy and W.B. Hubbard, Astroph. J. 213 (1977) 861.
[25] Y.Y. Kartavykh et al., Adv. Space Res. 38 (2006) 516.
[26] Y.Y. Kartavykh et al., Proceedings of the 30th ICRC, Mérida, México, 2007, Vol. 1, p. 79.
[27] J. Kiener et al., Astron. Astrophys. 445 (2006) 725.
[28] B. Klecker et al., Space Science Rev. 123 (2006) 217.
[29] B. Klecker et al., Space Science Rev. 124 (2006) 289.
[30] B. Klecker et al., Proceedings of the 30th ICRC, Mérida, México, 2007, Vol. 1, p. 83.
[31] K.L. Klein and G. Trottet, Space Science Rev. 95 (2001) 215.
[32] Y.K. Ko et al., J. Geophys. Res. 104 (1999) 17005.
[33] L. Kocharov et al., Astron. Astrophys. 357 (2000) 716.
[34] J. Kota, Proceedings of the 30th ICRC, Mérida, México, 2007, Vol. 1, p. 189.
[35] T. Kuwabara et al., Proceedings of the 30th ICRC, Mérida, México, 2007, Vol. 1, p. 335.
[36] T. Kuwabara et al., Proceedings of the 30th ICRC, Mérida, México, 2007, Vol. 1, p. 339.
[37] S.N. Kuznetsov et al., Proceedings of the 28th ICRC, Tsukuba,Japan, 2003, Vol. 6, p. 3183.
[38] S.N. Kuznetsov et al., Proceedings of the 30th ICRC, Mérida, México, 2007, Vol. 1, p. 71.
[39] S.N. Kuznetsov et al., Proceedings of the 30th ICRC, Mérida, México, 2007, Vol. 1, p. 121.
[40] A. Lara and R. Caballero-López, Proceedings of the 30th ICRC, Mérida, México, 2007, Vol. 1, p 299.
[41] R.A. Leske et al., Proceedings of the 30th ICRC, Mérida, México, 2007, Vol. 1, p. 375.
[42] G. Li et al., Proceedings of 30th ICRC Merida, Mexico, (2007), Id 1273.
[43] G. Li et al., Proceedings of 30th ICRC Merida, Mexico, (2007), Id 1281.
[44] G.M. Mason et al., Astrophys. J. 525 (1999) L133.
[45] G.M. Mason et al., Space Science Rev. 89 (1999) 327.
[46] Y. Matsubara et al., Proceedings of the 29th ICRC, Pune, India, 2005, Vol. 1, p. 17.
[47] Y. Matsubara et al., Proceedings of the 30th ICRC, Mérida, México, 2007, Vol. 1, p. 33.
[48] R.A. Mewaldt et al., Proceedings of the 30th ICRC, Mérida, México, 2007, Vol. 1, p. 99.
[49] R.A. Mewaldt et al., Proceedings of the 30th ICRC, Mérida, México, 2007, Vol. 1, p. 107.
[50] E. Möbius et al., Proceedings of the 28th ICRC, Tsukuba, Japan, 2003, Vol. 6, p. 3273.
[51] R. Müller-Mellin et al., Proceedings of the 30th ICRC, Mérida, México, 2007, Vol. 1, p. 371.
[52] G. Muñoz et al., Proceedings of 30th ICRC Merida, Mexico, (2007), Id 1245.
[53] Y. Muraki et al., Proceedings of the 30th ICRC, Mérida, México, 2007, Vol. 1, p. 29.

[54] C. K. Ng et al., Astrophys. J. 591 (2003) 461.
[55] E. Orlando et al., Proceedings of the 30th ICRC, Mérida, México, 2007, Vol. 1, p. 11.
[56] C. Pei et al., Astrophys. J. 641 (2006) 1222.
[57] J. Perez-Peraza et al., Proceedings of the 30th ICRC, Mérida, México, 2007, Vol. 1, p. 117.
[58] M.A. Popecki, AGU Geophysical Monograph 165 (2006) 115.
[59] B.R. Ragot and S.W. Kahler, Proceedings of the 30th ICRC, Mérida, México, 2007, Vol. 1, p. 147.
[60] D.V. Reames, Space Science Rev. 90 (1999) 413.
[61] I.G. Richardson and H.V. Cane, Proceedings of the 30th ICRC, Mérida, México, 2007, Vol. 1, p. 319.
[62] I.G. Richardson et al., Proceedings of the 30th ICRC, Mérida, México, 2007, Vol. 1, p. 323.
[63] J.M. Ryan et al., Proceedings of the 30th ICRC, Mérida, México, 2007, Vol. 1, p. 355.
[64] T. Sako et al., Proceedings of the 30th ICRC, Mérida, México, 2007, Vol. 1, p. 53.
[65] A. Struminski and I. Zimovets, Proceedings 30th ICRC, Mérida, México, 2007, Vol. 1, p. 7.
[66] E.V. Troitskaia and L. I. Miroshnichenko, Proceedings of the 30th ICRC, Mérida, México, 2007, Vol. 1, p. 23.
[67] E.V. Troitskaia et al., Sol. Phys. 242 (2007) 87.
[68] A.J. Tylka et al., in Acceleration and Transport of Energetic Particles Observed in the Heliosphere: ACE 2000 Symposium (ed. by R. A.Mewaldt et al., 2000), p. 147.
[69] A.J. Tylka et al., Astrophys.J. 625 (2005) 474.
[70] A.J. Tylka and M.A. Lee, Astrophys. J. 646 (2006) 1319.
[71] I.G. Usoskin et al., Proceedings of the 30th ICRC, Mérida, México, 2007, Vol. 1, p. 327.
[72] M. Vandas et al., Proceedings of the 30th ICRC, Mérida, México, 2007, Vol. 1, p. 191.
[73] G. Vedrenne et al., Astron. Astrophys. 411 (2003) L63.
[74] P.L. Verma, Proceedings of 30th ICRC Merida, Mexico, 2007, Id 546.
[75] T. T. Von Rosenvinge et al., Proceedings of the 30th ICRC, Mérida, México, 2007, Vol. 1, p. 103.
[76] K. Watanabe et al., Proceedings of the 30th ICRC, Mérida, México, 2007, Vol. 1, p. 41.
[77] A. Wawrzynczak and M. V. Alania, Proceedings of the 30th ICRC, Mérida, México, 2007, Vol. 1, p. 311.
[78] G. Wibberenz et al., Space Science Rev. 83 (1998) 309.
[79] M.E. Wiedenbeck et al., Proceedings of the 29th ICRC, Pune, India, 2005.
[80] M.E. Wiedenbeck et al., Proceedings of the 30th ICRC, Mérida, México, 2007, Vol. 1, p. 91.
[81] M.P. Yadav, Proceedings of 30th ICRC Merida, Mexico, 2007, Id 108.
[82] I. Zimovets, Proceedings of the 30th ICRC, Mérida, México, 2007, Vol. 1, p. 113.
[83] T.H. Zurbuchen and I.G. Richardson, Space Science Rev. 123 (2006) 31.